jove

Monitoring the Mechanical Evolution of Tissue During Neural Tube Closure of Chick Embryo

Chenjun Shi[1], **Chenchen Handler**[2], **Haden Florn**[1], **Jitao Zhang**[1]

[1] Department of Biomedical Engineering, College of Engineering, Wayne State University [2] Fischell Department of Bioengineering, University of Maryland

Corresponding Author

Jitao Zhang

zhang4@wayne.edu

Citation

Shi, C., Handler, C., Florn, H., Zhang, J. Monitoring the Mechanical Evolution of Tissue During Neural Tube Closure of Chick Embryo. *J. Vis. Exp.* (201), e66117, doi:10.3791/66117 (2023).

Date Published

November 10, 2023

DOI

10.3791/66117

URL

jove.com/video/66117

Abstract

Neural tube closure (NTC) is a critical process during embryonic development. Failure in this process can lead to neural tube defects, causing congenital malformations or even mortality. NTC involves a series of mechanisms on genetic, molecular, and mechanical levels. While mechanical regulation has become an increasingly attractive topic in recent years, it remains largely unexplored due to the lack of suitable technology for conducting mechanical testing of 3D embryonic tissue *in situ*. In response, we have developed a protocol for quantifying the mechanical properties of chicken embryonic tissue in a non-contact and non-invasive manner. This is achieved by integrating a confocal Brillouin microscope with an on-stage incubation system. To probe tissue mechanics, a pre-cultured embryo is collected and transferred to an on-stage incubator for *ex ovo* culture. Simultaneously, the mechanical images of the neural plate tissue are acquired by the Brillouin microscope at different time points during development. This protocol includes detailed descriptions of sample preparation, the implementation of Brillouin microscopy experiments, and data post-processing and analysis. By following this protocol, researchers can study the mechanical evolution of embryonic tissue during development longitudinally.

Introduction

Neural tube defects (NTDs) are severe birth defects of the central nervous system caused by failures in neural tube closure (NTC) during embryonic development[1]. The etiology of NTDs is complex. Studies have shown that NTC involves a sequence of morphogenetic processes, including convergent extension, bending of the neural plate (e.g., apical constriction), elevating the neural fold, and finally adhesion of the neural fold. These processes are regulated by multiple molecular and genetic mechanisms[2,3], and any malfunction in these processes may result in NTDs[4,5,6]. As mounting evidence suggests that mechanical cues also play crucial roles during NTC[3,7,8,9,10,11], and relationships have been found between genes and mechanical cues[12,13,14], it becomes imperative to investigate the tissue biomechanics during neurulation.

Several techniques have been developed for measuring the mechanical properties of embryonic tissues, including laser ablation (LA)[15], tissue dissection and relaxation (TDR)[16,17], micropipette aspiration (MA)[18], Atomic Force Microscopy (AFM)-based nanoindentation[19], microindenters (MI) and microplates (MP)[20], micro rheology (MR) with optical/magnetic tweezers[21,22,23], and droplet-based sensors[24]. Existing methods can measure mechanical properties at spatial resolutions ranging from subcellular to tissue scales. However, most of these methods are invasive because they require contact with the sample (e.g., MA, AFM, MI, and MP), external material injection (e.g., MR and droplet-based sensors), or tissue dissection (e.g., LA and TDR). As a result, it is challenging for existing methods to monitor the mechanical evolution of neural plate tissue *in situ*[25]. Recently, reverberant optical coherence elastography has shown promise for non-contact mechanical mapping with high spatial resolution[26].

Confocal Brillouin microscopy is an emerging optical modality that enables non-contact quantification of tissue biomechanics with subcellular resolution[27,28,29,30]. Brillouin microscopy is based on the principle of spontaneous Brillouin light scattering, which is the interaction between the incident laser light and the acoustic wave induced by thermal fluctuations within the material. Consequently, the scattered light experiences a frequency shift, known as the Brillouin shift ω_R, following the equation[31]:

$$\omega_B = 2n/\lambda \cdot \sqrt{M'/\rho} \cdot \sin\left(\frac{\theta}{2}\right) \quad (1)$$

Here, n is the refractive index of the material, λ is the wavelength of the incident light, M' is the longitudinal modulus, ρ is the mass density, and θ is the angle between the incident light and the scattered light. For the same type of biological materials, the ratio of refractive index and density $n/\sqrt{\rho}$ is approximately constant[28,32,33,34,35,36]. Thus, the Brillouin shift can be directly used to estimate relative mechanical changes in physiological processes. The feasibility of Brillouin microscopy has been validated in various biological samples[29,37,38]. Recently, time-lapse mechanical imaging of a live chick embryo was demonstrated by combining a Brillouin microscope with an on-stage incubation system[39]. This protocol provides detailed descriptions of sample preparation, experiment implementation, and data post-processing and analysis. We hope this effort will facilitate the widespread adoption of non-contact Brillouin technology for studying biomechanical regulation in embryo development and birth defects.

Protocol

The protocol has been approved by the Institutional Animal Care and Use Committee of Wayne State University.

1. Experimental preparation

1. Use a 70% ethanol solution to clean and sterilize the scissors and tweezers. Also, prepare disposable pipettes and a syringe.
2. Prepare a wash medium by adding 3.595 g of NaCl to 495 mL of deionized water. Then, add 5 ml of Penicillin-Streptomycin (5 U/mL) to the medium. Fill a 100 mm Petri dish with the wash medium and warm it to 37 °C.
3. Prepare culture dishes according to **Figure 1**, which illustrates the overall configuration.
    1. Prepare a piece of filter paper, cut it into a rectangular shape of approximately 17 mm × 20 mm, and remove the four corners. Create a hollow center in the filter paper, approximately 7 mm × 10 mm in size for securing the embryo (**Figure 1**, left).

NOTE: The collection of embryos is described in step 2.

2. Attach a commercial available ring (Φ = 1 inch, see **Table of Materials**) with a flexible film (i.e., paraffin film) layer, ensuring that the flexible film also has a hollow center. This ring with the film will be used to hold the filter paper with the embryo.

3. Finally, place the prepared ring into a 35 mm Petri dish (**Figure 1**, right).

   NOTE: The filter paper is for securing and holding the extracted embryo by placing the filter paper on the membrane and leaving the embryo in the center hollow area (which will be detailed in step 2). The four corners were cut to fit the size of the outside ring (not necessary if it is already fitted). A 35 mm glass-bottom culture dish is used for better laser beam propagation. The dish has an inner well (Φ = 23 mm), which can be filled with albumen for *ex ovo* culture. The diameter of the ring must be larger than the diameter of the inner well so that the well can be covered by the flexible film on the ring (**Figure 1**, inset). The size of the filter paper is not restricted and can be modified according to the size of the chosen ring and the culture dish. Alternatively, the bottom of the dish can be pre-coated with an agarose layer (thickness: ~1 mm). By removing agarose from the center of the layer using a blade, a well with a similar shape to the hollow center of the flexible film can be created for loading albumen. One critical point is that the four sides of the hollow filter paper need to have enough width (> 5 mm) to ensure the attachment of the embryo.

2. Extraction and *ex ovo* culture of the chicken embryo

NOTE: This step is modified from previously published reports[40,41].

1. After pre-culture, retrieve the egg from the incubator and place it on its long axis on the egg carton tray. Clean the eggshell with 70% ethanol, ensuring to cover the entire surface, and then allow it to rest for 15 min.

2. Hold the egg on its short axis and crack it at the bottom. Open the egg over a clean 100 mm Petri dish to extract its contents, as illustrated in **Figure 2**. Ensure not to rotate the egg while holding and cracking it.

3. Using a pipette, transfer and collect approximately 10 mL of the thin albumen (i.e., the liquid albumen[42]) into a 15 mL tube for *ex ovo* culture use. Fill the center well of the culture dish with the collected thin albumen (about 0.9 mL), as shown in **Figure 3**. The filling process should be slow, avoiding the formation of any bubbles inside the well. Ensure that the culture dish with albumen is warmed to 37 °C.

   NOTE: This dish will be used for culturing the embryo *ex ovo*. New culture dishes filled with wash medium will be used during Brillouin imaging (see step 3).

4. Using tissue paper, gently remove the thick albumen (i.e., viscous albumen) attached to the embryo by carefully separating the albumen from the vitelline membrane, as demonstrated in **Figure 4**. Avoid direct contact with the vitelline membrane.

5. After removing all the thick albumen, carefully affix the filter paper to the vitelline membrane. Ensure the body axis of the embryo aligns with the long axis of the center

rectangle on the filter paper. Use scissors to cut the membrane surrounding the filter paper.

6. Using tweezers, gently pull the isolated filter paper away from the yolk in an oblique direction. Flip the filter paper upside down to position the embryo with its dorsal side down (for inverted microscope configuration). Carefully immerse the entire filter paper from one side of the long axis into the 100 mm Petri dish with the wash medium in an oblique fashion.

7. Wash away any remaining yolk by gently spraying the wash medium parallel to the filter paper using a clean pipette. Avoid directly spraying the wash medium onto the membrane.

8. After clearing all the yolk, carefully remove the filter paper from the wash medium and use tissue paper to absorb any excess medium from the edges. Then, place the filter paper with the embryo onto the culture dish, ensuring that the dorsal side of the embryo is facing downward, as illustrated in **Figure 5**. To maintain humidity, place a moistened tissue paper in the dish.

9. Transfer the culture dish to the on-stage incubator for *ex ovo* culture.

3. Brillouin measurement of the embryo

1. Prepare another set of culture dishes and fill them with wash medium. Ensure the wash medium is warmed to 37 °C.

2. When the embryo reaches the desired developmental stage, transfer the filter paper with the embryo to the culture dish filled with wash medium. Place the culture dish into the on-stage incubator of the Brillouin microscope (see **Table of Materials**).

    1. Before conducting the Brillouin measurement, save a bright-field image of the entire embryo for reference. The detailed configuration of the Brillouin microscope has been previously described[30] and is summarized in the Results section (**Figure 6**).

3. Measure the Brillouin signal of water and methanol, which will be used in step 4 for the calibration process.

4. Adjust the incident laser power and electron-multiplying charge-coupled device (EMCCD, see **Table of Materials**) camera exposure time to achieve at least 10,000 counts of Brillouin signal. Using the bright-field image as a guide, set up the scan range and step size. Acquire a Brillouin image of the region of interest by scanning the embryo using a 2D translational stage.
NOTE: The horizontal scanning range can be determined based on the bright-field image, and the vertical (i.e., depth) scanning range can be determined based on the signal strength obtained from a quick and coarse scan. To prevent any photodamage to the embryo, limit the incident power to 25 mW, and set the exposure time of the EMCCD camera to 50 ms. Choose a step size of 2 µm in the horizontal direction and 1 µm in the vertical direction to balance imaging quality and acquisition time.

5. After completing the scan, carefully remove the filter paper with the embryo and use tissue paper to absorb any excess wash medium. Then, place the filter paper back into the culture dish filled with thin albumen for continuous culturing in the on-stage incubator.

6. Repeat steps 3.2-3.5 at regular time intervals (e.g., 1.5 h) to capture time-lapse Brillouin images as the embryo develops.

7. Reconstruct the 2D Brillouin image following step 4.

4. Brillouin image reconstruction

1. Calibrate the Brillouin spectrometer using Brillouin signals of water and methanol to calculate the free spectral range (FSR) and the pixel-to-frequency conversion ratio (PR) of the spectrometer[30]. The calibrated values of FSR and PR will be used to calculate the Brillouin shift of the embryo at each pixel.

   NOTE: **Figure 7A** displays a raw Brillouin spectrum captured by the EMCCD camera. By vertically summing the spectrum and then doing a Lorentzian fitting, the peak distance Δd of the two dots can be obtained (**Figure 7B**). By getting the peak distance of water Δd_{water} and methanol $\Delta d_{methanol}$, the FSR and PR can be computed based on the equations[30]: $PR = 2\cdot(\omega_{methanol}-\omega_{water})/(\Delta d_{water}- \Delta d_{methanol})$, and $FSR = 2\cdot\omega_{water} + PR\cdot\Delta d_{water}$, with the known Brillouin shift of water ω_{water} = 6.01 GHz and methanol $\omega_{methanol}$ = 4.49 GHz at 660 nm.

2. Obtain the peak distance of the Brillouin signal at each pixel of the sample. Calculate the Brillouin shift based on the calibrated FSR and PR: $\omega_{sample} = 0.5 (FSR - PR \times \Delta d_{sample})$[30], where ω_{sample} is the Brillouin shift of the sample, and Δd_{sample} is the peak distance of the Brillouin signal.

3. Reconstruct the 2D Brillouin image based on the Brillouin shifts of all pixels.

   NOTE: To conduct local analysis, one can select a region of interest (e.g., the neural plate) from the acquired Brillouin image and quantify its mechanical properties. A common approach is to calculate the average Brillouin shift of the selected region.

Representative Results

Figure 6 shows the schematic of the Brillouin microscope. The system employs a 660 nm laser as the light source. An isolator is placed right after the laser head to reject any back-reflected light, and a neutral density (ND) filter is used to adjust the laser power. A pair of lenses, L1 and L2, with focal lengths of f1 = 16 mm and f2 = 100 mm, respectively, are used to expand the laser beam. A half-wave plate (HWP) and a linear polarizer (Polarizer 1) are employed to adjust the power of the beam shining on either the sample or the calibration materials (i.e., water and methanol) after the polarized beam splitter (PBS). To focus the laser into the sample and collect backward scattered light, an objective lens (OBJ2) with a numerical aperture (NA) of 0.6 and a magnification of 40 are used. The incident light and backward scattered light are separated by the same PBS after polarization adjustment using a quarter-wave plate (QWP2). Similarly, OBJ1 and QWP1 are used to guide the laser beam to the calibration materials. The Brillouin signal is delivered by a single-mode fiber to a Brillouin spectrometer[43] for analysis. Inside the spectrometer, a cylindrical lens (C1) couples the Brillouin signal into the first VIPA (virtually imaged phased array) etalon. The output of the first VIPA etalon is reshaped by another cylindrical lens (C2) and focused onto Mask 1 to reject non-scattered laser light. Then, the Brillouin signal is coupled into a second VIPA etalon by a spherical lens (SL1), reshaped by another spherical lens (SL2), and projected onto Mask 2. The resulting spectral pattern then goes through a 4-f unit for noise rejection and is projected onto an EMCCD for recording. We used a commercial microscope body (see **Table of Materials**). Generally, any microscope body with different brands can be used as long as it has an available port for delivering the external light beam. The on-stage incubator

is a metal chamber with temperature, gas, and air flow control. The position of the sample is adjusted *via* the 2D motorized stage. A complementary metal-oxide semiconductor (CMOS) camera is used to acquire the bright-field image.

Figure 8 shows the time-lapse bright-field and Brillouin images of a representative chicken embryo. The embryo was extracted after 29 h of *in ovo* culture, and the images were taken at 29 h, 30.5 h, and 32 h with *ex ovo* culture, which corresponds to somite numbers of 4, 5, and 8, respectively[44]. In general, the embryo can be cultured in the on-stage incubator for at least 24 h. The red line in the bright-field image indicates the location for Brillouin imaging. With the acquired Brillouin images, the neural plate region was selected (highlighted by the black dotted line in **Figure 8**) and calculated the average Brillouin shift of this region. As shown in **Figure 9**, the averaged Brillouin shift of the tissue increases during neural tube closure. The longitudinal modulus is also calculated based on equation (1), where the value of $n/\sqrt{\rho}$ = 1.3330 is estimated from literature using zebrafish embryos[45], assuming the value is relatively constant for similar kinds of biological tissues[28,33].

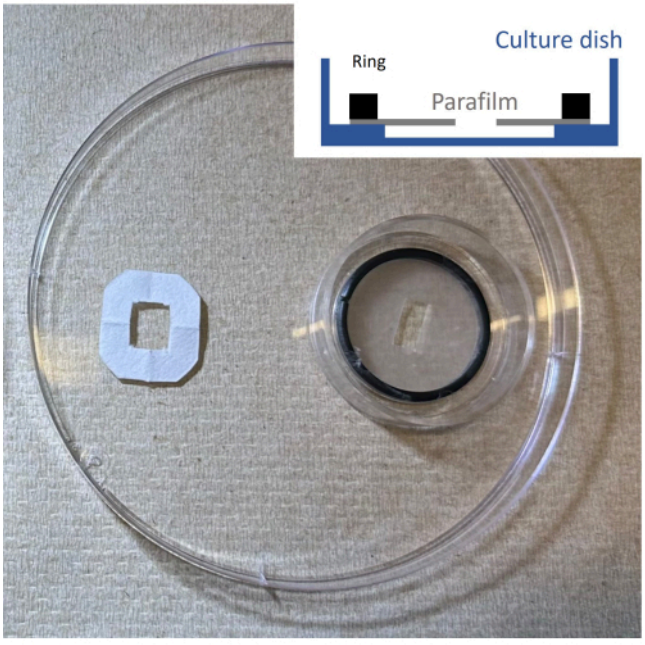

Figure 1: Schematic of the whole culture dish configuration for embryonic development. This figure shows a filter paper for attaching the embryo on the left and a 35 mm culture dish with a ring attached with a flexible film layer on the right. The cross-section schematic is also provided. Please click here to view a larger version of this figure.

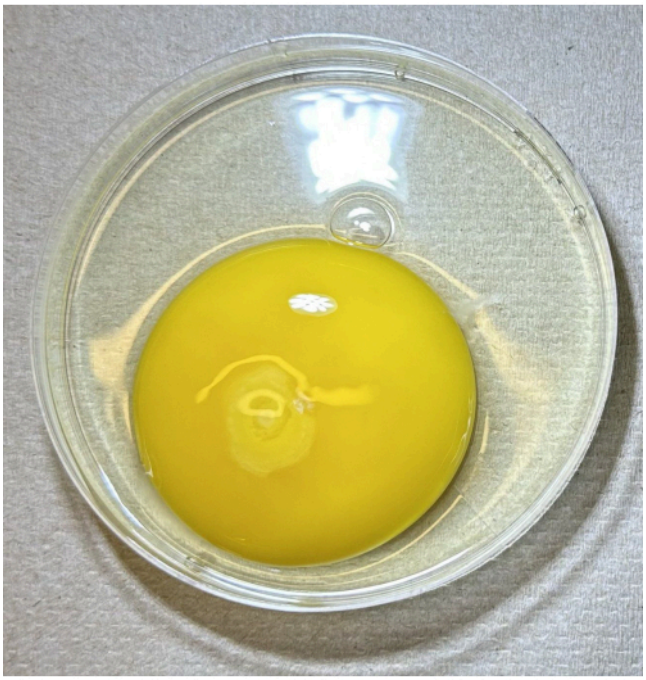

Figure 2: The process of opening the eggshell above a clean 100 mm Petri dish to extract the egg into the dish.

Please click here to view a larger version of this figure.

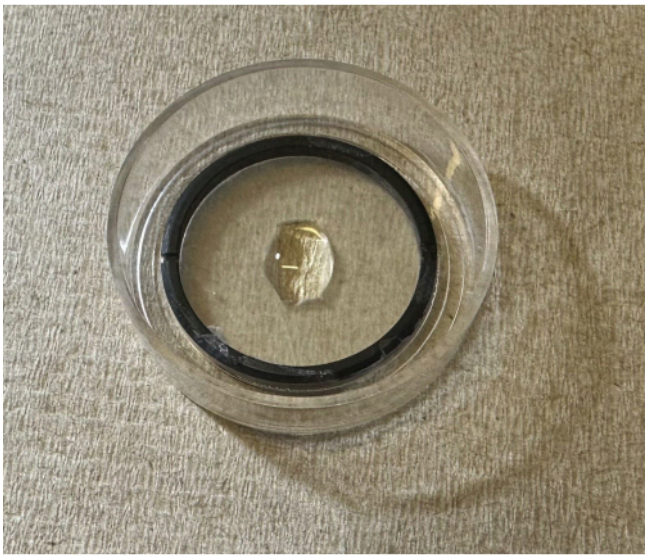

Figure 3: Filling the center well of the culture dish with thin albumen. Please click here to view a larger version of this figure.

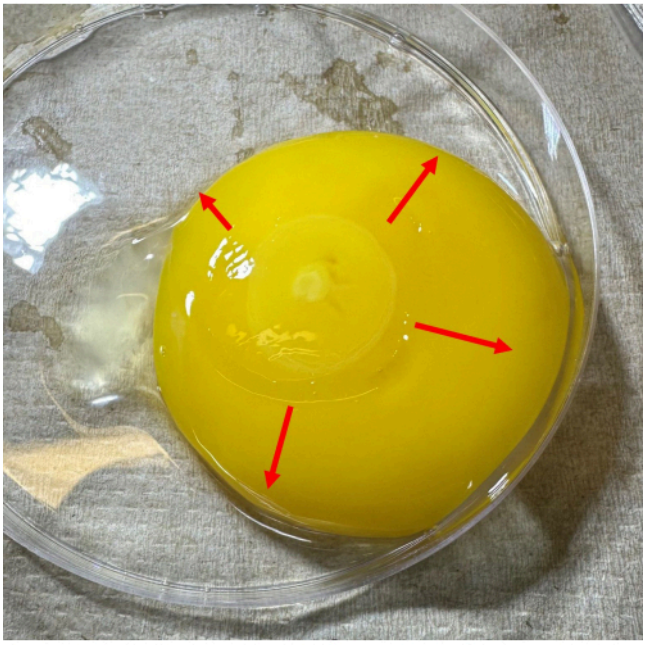

Figure 4: Dragging away the thick albumen in the direction indicated by the red arrow, using a piece of tissue paper. Please click here to view a larger version of this figure.

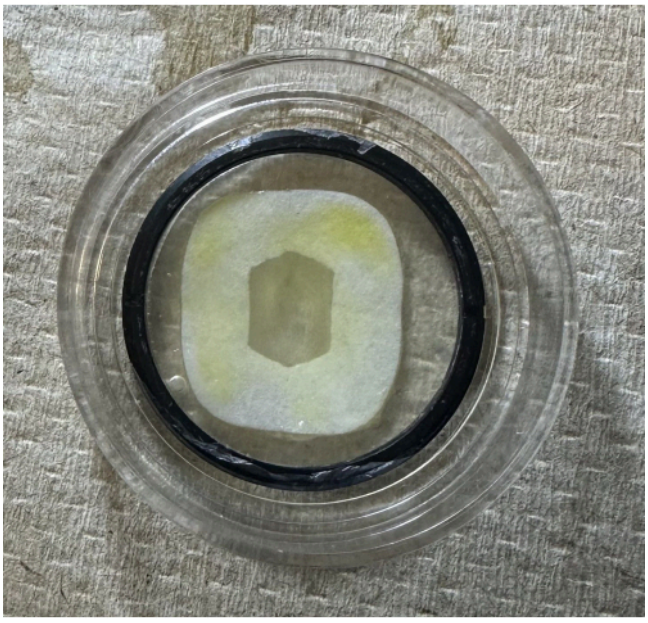

Figure 5: The placement of the filter paper into the culture dish with the embryo on the upside of the filter paper.

Please click here to view a larger version of this figure.

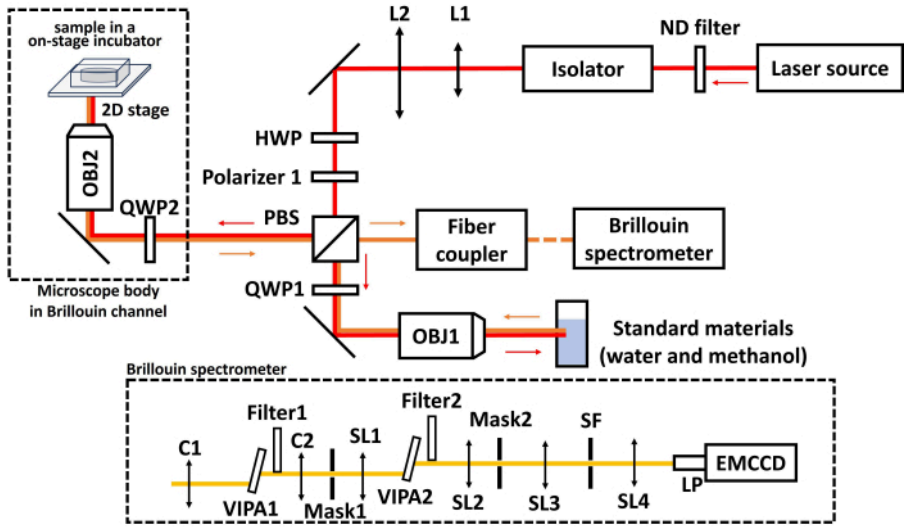

Figure 6: Schematic of the Brillouin microscope. The red arrow indicates the light path of the laser beam, and the orange arrow indicates the light path of the Brillouin signal. L1, L2, SL1-SL4: spherical lens; SF: spatial filter; C1, C2: cylindrical lens, HWP: half-wave plate; PBS: polarized beam splitter; QWP1, QWP2: quarter-wave plate; OBJ1, OBJ2: Objective lens; LP: lens pair. VIPA: virtually imaged phased array. Please click here to view a larger version of this figure.

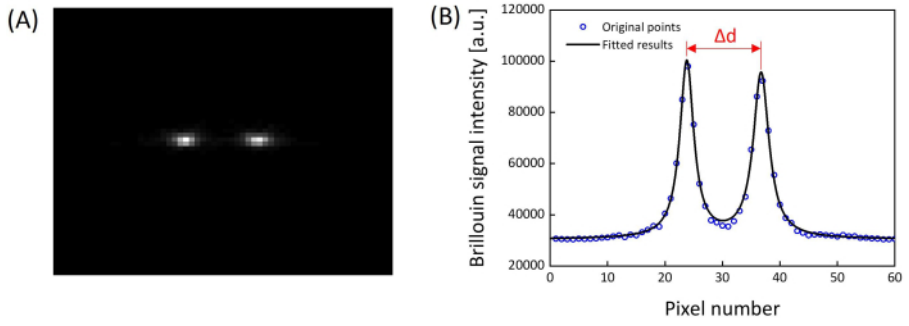

Figure 7: Representative Brillouin signal. (**A**) A representative Brillouin spectrum captured by the EMCCD. (**B**) A vertically summed Brillouin spectrum and corresponding Lorentzian fitting result. Please click here to view a larger version of this figure.

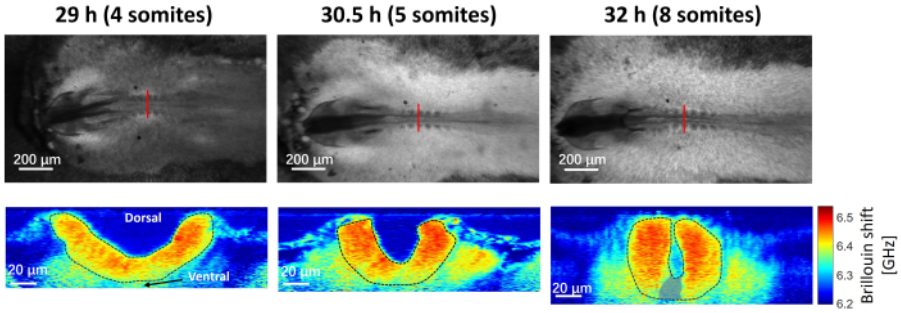

Figure 8: Bright field images and the corresponding Brillouin cross-section images of the embryo at 29 h, 30.5 h and 32 h with 4, 5 and 8 somites. Red solid lines indicate the location for Brillouin imaging, and the black dotted line indicate the neural plate region. The grey area in 32 h (8 somites) image is an artifact of curve fitting due to the weak Brillouin signal and is excluded when calculating the average shift. Please click here to view a larger version of this figure.

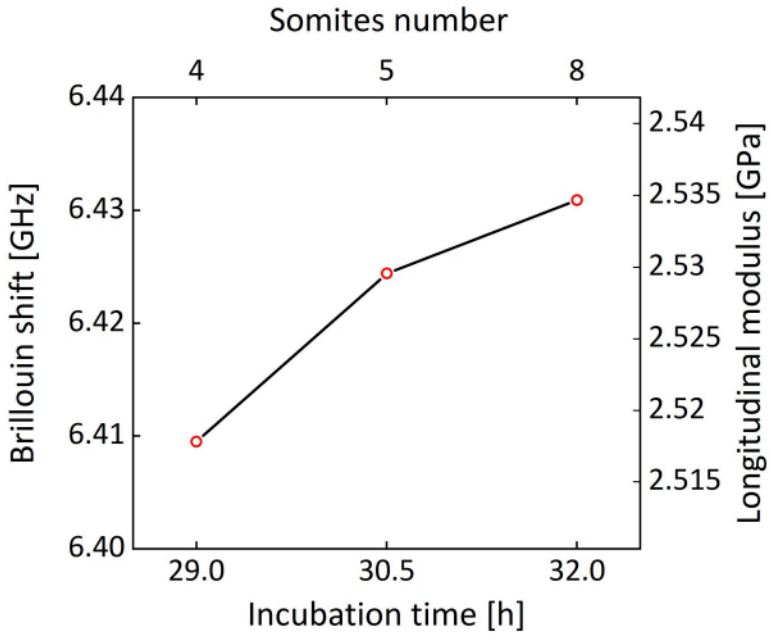

Figure 9: Brillouin shift and the estimated longitudinal modulus of the neural plate against somite number and incubation time. Please click here to view a larger version of this figure.

Discussion

The early development of the embryo can be easily affected by external disturbances. Therefore, utmost caution is required during the sample extraction and transfer. One potential issue is the detachment of the embryo from the filter paper, which can lead to the shrinking of the vitelline membrane and result in a tilted artifact of the neural plate in Brillouin imaging. Furthermore, this shrinking may halt the development of the embryo. Attention should be paid to several critical steps to prevent detachment. First, in step 2.4, it is crucial to ensure thorough removal of albumen from the membrane surface. Any remaining albumen can impede the proper adhesion of the membrane to the filter paper[46,47]. Additionally, during the washing process, it is important to spray the washing medium in a direction parallel to the membrane. Directly hitting the membrane with the liquid flow may cause detachment or even tear the membrane. Furthermore, the entire washing process should be completed within a short time (e.g., <3 min), as prolonged immersion can also lead to detachment of the embryo from the filter paper.

Before conducting Brillouin measurements, it is necessary to transfer the embryo to a dish with wash medium. This is because the Brillouin shift of the albumen is very close to the neural plate tissues, causing poor image contrast. Brillouin imaging is obtained by point scanning, which can be time-consuming, especially when dealing with many points. In this protocol, the scanning region is approximately 400 µm horizontally and less than 100 µm vertically. To avoid disturbance to the embryo's development, the total acquisition time was limited to within 30 min. This is achieved by utilizing a step size of 2 µm horizontally and 1 µm vertically. In case one is only interested in the average Brillouin shift of a specific region, a quick and coarse scan (e.g., with a step size of 4 µm both horizontally and vertically) can be implemented, which will take less than 5 min and can mitigate the negative impact on embryo development.

Brillouin microscopy offers a real-time and non-invasive imaging approach for investigating the biomechanics of embryo development. One limitation of this method lies in its penetration depth, which is about 100-200 µm depending on the embryo's development stage. While increasing the laser power and/or exposure time of the EMCCD can partially address this issue, it comes at the cost of potential phototoxicity and/or a long acquisition time. Alternatively, existing optical technologies, such as adaptive optics, could be potentially employed to improve the penetration depth[48].

In conclusion, we have established a protocol for probing the mechanical properties of live chicken embryos using Brillouin microscopy. This non-contact method can fulfill current unmet needs and is complementary to other existing tools for studying biomechanics in embryonic development.

Disclosures

The authors declare that they have no conflict of interest.

Acknowledgments

This work is supported by the Eunice Kennedy Shriver National Institute of Child Health and Human Development, National Institutes of Health (K25HD097288, R21HD112663).

References

1. Greene, N. D. E. Copp, A. J. Neural tube defects. *Annual Review of Neuroscience.* **37** (1), 221-242 (2014).
2. Suzuki, M., Morita, H., Ueno, N. Molecular mechanisms of cell shape changes that contribute to vertebrate neural

tube closure. *Development, Growth & Differentiation.* **54** (3), 266-276 (2012).

3. Nikolopoulou, E., Galea, G. L., Rolo, A., Greene, N. D. E., Copp, A. J. Neural tube closure: Cellular, molecular and biomechanical mechanisms. *Development.* **144** (4), 552-566 (2017).
4. Juriloff, D. M. Harris, M. J. Mouse models for neural tube closure defects. *Human Molecular Genetics.* **9** (6), 993-1000 (2000).
5. Copp, A. J., Greene, N. D. E. Genetics and development of neural tube defects. *The Journal of Pathology: A Journal of the Pathological Society of Great Britain and Ireland.* **220** (2), 217-230 (2010).
6. Wang, M., De Marco, P., Capra, V., Kibar, Z. Update on the role of the non-canonical wnt/planar cell polarity pathway in neural tube defects. *Cells.* **8** (10), 1198 (2019).
7. Galea, G. L. et al. Biomechanical coupling facilitates spinal neural tube closure in mouse embryos. *Proceedings of the National Academy of Sciences.* **114** (26), E5177-E5186 (2017).
8. Moon, L. D., Xiong, F. Mechanics of neural tube morphogenesis. *Seminars in Cell & Developmental Biology.* **130**, 56-69 (2022).
9. Christodoulou, N., Skourides, P. A. Distinct spatiotemporal contribution of morphogenetic events and mechanical tissue coupling during xenopus neural tube closure. *Development.* **149** (13), dev200358 (2022).
10. De Goederen, V., Vetter, R., Mcdole, K., Iber, D. Hinge point emergence in mammalian spinal neurulation. *Proceedings of the National Academy of Sciences.* **119** (20), e2117075119 (2022).
11. Christodoulou, N., Skourides, P. A. Somitic mesoderm morphogenesis is necessary for neural tube closure during xenopus development. *Frontiers in Cell and Developmental Biology.* **10**, 1091629 (2023).
12. Nikolopoulou, E. et al. Spinal neural tube closure depends on regulation of surface ectoderm identity and biomechanics by grhl2. *Nature Communications.* **10** (1), 2487 (2019).
13. Nychyk, O. et al. Vangl2-environment interaction causes severe neural tube defects, without abnormal neuroepithelial convergent extension. *Disease Models & Mechanisms.* **15** (1), dmm049194 (2022).
14. Li, B., Brusman, L., Dahlka, J., Niswander, L. A. Tmem132a ensures mouse caudal neural tube closure and regulates integrin-based mesodermal migration. *Development.* **149** (17), dev200442 (2022).
15. Zulueta-Coarasa, T., Fernandez-Gonzalez, R. Laser ablation to investigate cell and tissue mechanics in vivo. *Integrative Mechanobiology: Micro-and Nano Techniques in Cell Mechanobiology.* 128-147. Cambridge University Press. (2015).
16. Wiebe, C., Brodland, G. W. Tensile properties of embryonic epithelia measured using a novel instrument. *Journal of Biomechanics.* **38** (10), 2087-2094 (2005).
17. Luu, O., David, R., Ninomiya, H., Winklbauer, R. Large-scale mechanical properties of xenopus embryonic epithelium. *Proceedings of the National Academy of Sciences.* **108** (10), 4000-4005 (2011).
18. Maître, J. L., Niwayama, R., Turlier, H., Nédélec, F., Hiiragi, T. Pulsatile cell-autonomous contractility drives compaction in the mouse embryo. *Nature Cell Biology.* **17** (7), 849-855 (2015).

19. Krieg, M. et al. Tensile forces govern germ-layer organization in zebrafish. *Nature Cell Biology.* **10** (4), 429-436 (2008).
20. Zamir, E. A., Srinivasan, V., Perucchio, R., Taber, L. A. Mechanical asymmetry in the embryonic chick heart during looping. *Annals of Biomedical Engineering.* **31**, 1327-1336 (2003).
21. Bambardekar, K., Clément, R., Blanc, O., Chardès, C., Lenne, P. F. Direct laser manipulation reveals the mechanics of cell contacts in vivo. *Proceedings of the National Academy of Sciences.* **112** (5), 1416-1421 (2015).
22. Savin, T. et al. On the growth and form of the gut. *Nature.* **476** (7358), 57-62 (2011).
23. Almonacid, M. et al. Active diffusion positions the nucleus in mouse oocytes. *Nature Cell Biology.* **17** (4), 470-479 (2015).
24. Campàs, O. et al. Quantifying cell-generated mechanical forces within living embryonic tissues. *Nature Methods.* **11** (2), 183-189 (2014).
25. Campàs, O. A toolbox to explore the mechanics of living embryonic tissues. *Seminars in Cell & Developmental Biology.* **55**, 119-130 (2016).
26. Christian, Z. D. et al. High-resolution 3D biomechanical mapping of embryos with reverberant optical coherence elastography (Rev-OCE). *Proceedings of SPIE.* 123670P, doi.org/10.1117/12.2650904 (2023).
27. Scarcelli, G., Yun, S. H. J. N. P. Confocal brillouin microscopy for three-dimensional mechanical imaging. *Nature Photonics.* **2** (1), 39-43 (2008).
28. Scarcelli, G. et al. Noncontact three-dimensional mapping of intracellular hydromechanical properties by brillouin microscopy. *Nature Methods.* **12** (12), 1132-1134 (2015).
29. Prevedel, R., Diz-Muñoz, A., Ruocco, G., Antonacci, G. Brillouin microscopy: An emerging tool for mechanobiology. *Nature Methods.* **16** (10), 969-977 (2019).
30. Zhang, J., Scarcelli, G. Mapping mechanical properties of biological materials via an add-on brillouin module to confocal microscopes. *Nature Protocols.* **16** (2), 1251-1275 (2021).
31. Boyd, R. W. *Nonlinear optics.* Academic press, doi.org/10.1016/C2015-0-05510-1 (2020).
32. Scarcelli, G., Kim, P., Yun, S. H. *In vivo* measurement of age-related stiffening in the crystalline lens by brillouin optical microscopy. *Biophysical Journal.* **101** (6), 1539-1545 (2011).
33. Scarcelli, G., Pineda, R., Yun, S. H. Brillouin optical microscopy for corneal biomechanics. *Investigative Ophthalmology & Visual Science.* **53** (1), 185-190 (2012).
34. Antonacci, G., Braakman, S. Biomechanics of subcellular structures by non-invasive brillouin microscopy. *Scientific Reports.* **6** (1), 37217 (2016).
35. Zhang, J. et al. Tissue biomechanics during cranial neural tube closure measured by brillouin microscopy and optical coherence tomography. *Birth Defects Research.* **111** (14), 991-998 (2019).
36. Zhang, J. et al. Nuclear mechanics within intact cells is regulated by cytoskeletal network and internal nanostructures. *Small.* **16** (18), 1907688 (2020).
37. Elsayad, K., Polakova, S., Gregan, J. Probing mechanical properties in biology using brillouin

microscopy. *Trends in Cell Biology.* **29** (8), 608-611 (2019).

38. Poon, C., Chou, J., Cortie, M., Kabakova, I. Brillouin imaging for studies of micromechanics in biology and biomedicine: From current state-of-the-art to future clinical translation. *Journal of Physics: Photonics.* **3** (1), 012002 (2020).
39. Handler, C., Scarcelli, G., Zhang, J. Time-lapse mechanical imaging of neural tube closure in live embryo using brillouin microscopy. *Scientific Reports.* **13** (1), 263 (2023).
40. Chapman, S. C., Collignon, J., Schoenwolf, G. C., Lumsden, A. Improved method for chick whole-embryo culture using a filter paper carrier. *Developmental dynamics: an official publication of the American Association of Anatomists.* **220** (3), 284-289 (2001).
41. Schmitz, M., Nelemans, B. K. A., Smit, T. H. A submerged filter paper sandwich for long-term ex ovo time-lapse imaging of early chick embryos. *Journal of Visualized Experiments.* **118**, e54636 (2016).
42. Nys, Y., Guyot, N. in *Improving the safety and quality of eggs and egg products, vol 1: Egg chemistry, production and consumption.* eds Nys, Y., Bain, M., VanImmerseel, F. 83-132 (2011).
43. Berghaus, K. V., Yun, S. H., Scarcelli, G. High speed sub-ghz spectrometer for brillouin scattering analysis. *Journal of Visualized Experiments.* **106**, e53468 (2015).
44. Hamburger, V., Hamilton, H. L. A series of normal stages in the development of the chick embryo. *Journal of Morphology.* **88** (1), 49-92 (1951).
45. Schlüßler, R. et al. Mechanical mapping of spinal cord growth and repair in living zebrafish larvae by brillouin imaging. *Biophysical Journal.* **115** (5), 911-923 (2018).
46. Williams, R. M., Sauka-Spengler, T. Ex ovo electroporation of early chicken embryos. *STAR Protocols.* **2** (2), 100424 (2021).
47. Chapman, S. C., Collignon, J., Schoenwolf, G. C., Lumsden, A. Improved method for chick whole-embryo culture using a filter paper carrier. *Developmental Dynamics.* **220** (3), 284-289 (2001).
48. Edrei, E., Scarcelli, G. Adaptive optics in spectroscopy and densely labeled-fluorescence applications. *Optics Express.* **26** (26), 33865-33877 (2018).